(11) Rossi, P; McCreery, R. L., J. Electroanal. Chem. Interfacial Electrochem. 1983, 151, 47–64.
(12) Jan, C. C.; Lavine, B. K.; McCreery, R. L. Anal. Chem. 1985, 57, 752–758.
(13) Klein, Miles V. Optics; John Wiley: New York, 1970; Chapter 7.
(14) McCreery, R. L.; Pruiksma, R.; Fagan, R. Anal. Chem. 1979, 51, 749–752.
(15) Ruzicka, J.; Hansen, E. H. Anal. Chim. Acta 1980, 114, 21.
(16) Landrum, H. L.; Salmon, R. T.; Hawkridge, F. M. J. Am. Chem. Soc. 1977, 99, 3154–3158.
(17) Newman, J. In Electroanalytical Chemistry; Marcel Dekker; New York, 1973; Vol. 6.
(18) Tobias, C. W.; Eisenberg, M.; Wilke, C. R. J. Electrochem. Soc. 1952, 99, 359C–365C.
(19) Rossi, P. Ph.D. Thesis, The Ohio State University, 1982.
(20) Yeung, E. S.; Synovec, R. Anal. Chem. 1986, 58, 1237A–1256A.

RECEIVED for review September 23, 1988. Accepted March 9, 1989. This work was supported by grants from the Denison University Research Foundation and the Denison University Faculty Development Program.

Scanning Electrochemical Microscopy. Theory of the Feedback Mode

Juhyoun Kwak and Allen J. Bard*

Department of Chemistry, The University of Texas, Austin, Texas 78712

The steady-state current that flows between the scanning tip (a disk ultramicroelectrode imbedded in an insulating sheath) and a planar sample substrate in a scanning electrochemical microscope (SECM) operating in the feedback mode is calculated by the finite element method with an exponentially expanding grid, for both conductive and insulating samples. For conductive substrates the tip current, representing, for example, the oxidation reaction of R to O, is enhanced by flow of R generated at the substrate to the tip and is a function of tip/substrate distance, *d*, but not the radius of the insulating sheath. For insulating substrates, the tip current is decreased by blockage of the diffusion of R to the tip by the substrate and depends upon *d* and the insulating sheath radius. The theoretical results are compared to experimental studies.

INTRODUCTION

A previous paper from our group described the principles of the scanning electrochemical microscope (SECM) and its operation in the feedback mode (*1*). In the SECM faradaic currents at an ultramicroelectrode tip (diameter ca. micrometers) are measured as the tip is moved near the surface of a sample immersed in an electrolyte solution. The tip current, i_T, is controlled by electrochemical reactions at the tip and sample and is a function of the tip/sample distance, d, and the conductivity and chemical nature of the sample. The measurement of i_T can thus provide information about sample topography (variable resolution depending on the size of tip electrode) and its electrical and chemical properties. In our earlier paper (*1*) a model for calculating i_T for a conductive substrate was given based on a thin layer cell approximation combined with the steady-state current that flows to a microdisk electrode. In this paper we develop a more rigorous steady-state model for both conductive and insulating substrates and carry out simulations that provide working curves of i_T as a function of d and tip radius.

The basic principles of operation of the SECM are given in Figure 1. For example, a species O in solution at a concentration C_O^* and with a diffusion coefficient, D_O, is reduced to species R in an n-electron reaction at the tip. The current at the tip is a function of the flux of O to the tip. When the tip is far from any surface (Figure 1A), the steady-state current to the imbedded disk is given by the well-known expression (*2*, *3*)

$$i = 4nFD_OC_O^*a \quad (1)$$

When the tip is near a conductive substrate (Figure 1B), which is at a potential where R is oxidized to O, the additional flux of O to the tip (termed the feedback current) (1) will cause i_T to be larger than that given by eq 1. On the other hand, when the tip is near an insulating substrate (Figure 1C), diffusion of O to the tip is partially blocked and i_T is smaller than that in eq 1. A calculation of the magnitude of i_T thus depends upon solving the equations for steady-state diffusion of O and R between tip and substrate. The rather complex disk/plane geometry involved prevents the derivation of a closed-form solution, and digital simulations were used to obtain concentration profiles and working curves of i_T vs d. Instead of the well-known finite difference method (FDM) often used in electrochemical diffusion calculations (*4*, *5*), the finite element method (FEM), which is widely employed simulation approach in engineering studies (*6*, *7*), was used. To solve the two-dimensional (axisymmetric) steady-state electrochemical diffusion problem, it was convenient to use the FEM source programs for axisymmetric steady-state heat conduction, which are of the same mathematical form as those for mass transfer, and are described in detail in textbooks in engineering science (*6*, *7*). The well-known exponentially expanding grid method (*8–10*) was used to generate a reasonable two-dimensional grid (see Appendix) according to the principle that the regions of steeper concentration gradient region require more grid points than the other regions. The application of the FEM with two-dimensional expanding grid method (*8–10*) allowed calculations to be carried out with practical computer memories and reasonable execution times. The simulated currents were compared to experimental ones with both conductive and insulating substrates and the agreement is shown to be satisfactory. This demonstrates that measurement of i_T at a tip of known radius can be used to determine the tip/substrate distance, d, and that scans of the tip over the substrate surface can provide absolute topographic information.

EXPERIMENTAL SECTION

The apparatus and experimental techniques have been described previously (*1*). All experiments here utilized a 5 μm radius

0003-2700/89/0361-1221$01.50/0 © 1989 American Chemical Society

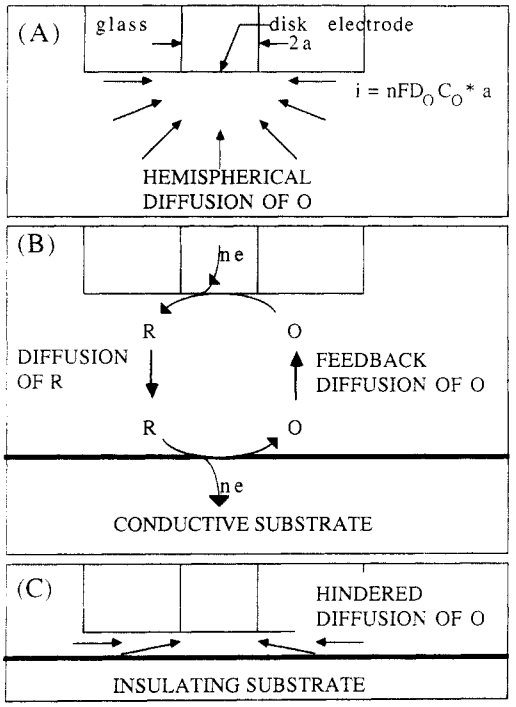

Figure 1. Basic principles of scanning electrochemical microscopy (SECM): (A) far from substrate, (B) near a conductive substrate, (C) near an insulating substrate.

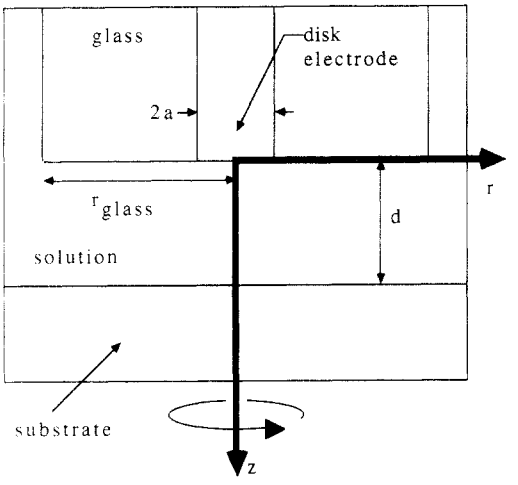

Figure 2. Disk electrode and planar substrate in axisymmetric system.

Pt disk imbedded in glass as a tip. Solutions were 2.5 mM ferrocene in acetonitrile containing 25 mM tetra-*n*-butylammonium fluoroborate (TBABF4).

FORMULATION OF MODEL

We consider the oxidation reaction R – ne^- → O at the tip and calculate the steady-state concentrations of O and R, $C_O(r,z)$ and $C_R(r,z)$, respectively, for the axisymmetric arrangement shown in Figure 2. The electrochemical mass transfer problem can be represented by the second-order partial differential diffusion equations

$$D_O\{\partial^2 C_O(r,z)/\partial r^2 + (1/r) \times [\partial C_O(r,z)/\partial r] + \partial^2 C_O(r,z)/\partial z^2\} = 0 \quad (2)$$

$$D_R\{\partial^2 C_R(r,z)/\partial r^2 + (1/r) \times [\partial C_R(r,z)/\partial r] + \partial^2 C_R(r,z)/\partial z^2\} = 0 \quad (3)$$

A list of all symbols is given in Table I. The boundary conditions that apply to this problem, with the assumption that $r_{glass} \gg a$ (where r_{glass} is the radius of the glass sheath surrounding the disk electrode), are as follows: For the disk electrode ($z = 0$ and $0 \le r \le a$)

$$C_O(r,0)/C_R(r,0) = \exp\{(nF/RT)(E_d - E^{\circ\prime})\} \quad (4)$$

$$D_O[\partial C_O(r,z)/\partial z]_{z=0} + D_R[\partial C_R(r,z)/\partial z]_{z=0} = 0 \quad (5)$$

where E_d is the potential applied to the disk electrode. At the glass surrounding the disk ($z = 0$ and $a \le r \le r_{glass}$)

$$[\partial C_O(r,z)/\partial z] = [\partial C_R(r,z)/\partial z] = 0 \quad (6)$$

The semiinfinite conditions ($r \ge r_{glass}$ for $0 < z < d$) are

Table I

symbol	usual dimensions	meaning
i_T	A, nA	current at the tip electrode
d	cm, μm	distance between tip and substrate
D_O	cm^2/s	diffusion coefficient of oxidized species
C_O*	M, mM	bulk concentration of oxidized species
D_R	cm^2/s	diffusion coefficient of reduced species
C_R*	M, mM	bulk concentration of reduced species
z	cm, μm	normal distance from disk electrode
r	cm, μm	radial distance from the center of disk electrode
$C_O(r,z)$	M, mM	steady-state concentration of oxidized species at location r,z
$C_R(r,z)$	M, mM	steady-state concentration of reduced species at location r,z
a	cm, μm	radius of disk electrode
r_{glass}	cm, μm	radius of the glass sheath surrounding the disk electrode
n	none	electrons per molecule oxidized and reduced
F	C	faradaic constant
R	J mol^{-1} K^{-1}	gas constant
T	K	temperature
E_d	V	potential of disk electrode
$E^{\circ\prime}$	V	formal potential of a redox couple
E_s	V	potential of a conductive substrate
E_{eq}	V	equilibrium potential of the solution
j	none	nodal point index of element domain (e)
j'	none	nodal point index of global space domain
FCO$^{(e)}(R,Z)$	none	functional form of the fractional concentration of oxidized species in element domain (e)
FCO(R,Z)	none	functional form of the fractional concentration of oxidized species in global space domain
FCO$^{(e)}(R_j,Z_j)$	none	fractional concentration of oxidized species at node j of element domain (e)
FCO$(R_{j'},Z_{j'})$	none	fractional concentration of oxidized species at global node j'
FCR$^{(e)}(R,Z)$	none	functional form of the fractional concentration of reduced species in element domain (e)
FCR(R,Z)	none	functional form of the fractional concentration of reduced species in global space domain
FCR$^{(e)}(R_j,Z_j)$	none	fractional concentration of reduced species at node j of element domain (e)
FCR$(R_{j'},Z_{j'})$	none	fractional concentration of reduced species at global node j'
$N_j^{(e)}(R,Z)$	none	interpolation polynomials of element (e) (nonzero only inside element (e), 1 at node j and 0 at other nodes)
$N_{j'}(R,Z)$	none	global interpolation polynomials (nonzero only adjacent elements domain, 1 at node j' and 0 at other adjacent nodes)

$$C_O(r,z) = C_O^* \quad (7)$$

$$C_R(r,z) = C_R^* \quad (8)$$

$$[\partial C_O(r,z)/\partial z] = [\partial C_R(r,z)/\partial z] = 0 \quad (9)$$

$$[\partial C_O(r,z)/\partial r] = [\partial C_R(r,z)/\partial r] = 0 \quad (10)$$

We choose the above approximate semiinfinite boundary conditions, eq 7–10, for simplicity; rigorous consideration of the diffusion at $r > r_{glass}$ may be required, especially when r_{glass} is small, for more accurate simulations. At the planar sample (substrate) surface ($z = d$ and $r \geq 0$) the boundary conditions depend upon the conductivity of the substrate. For a conductive substrate

$$C_O(r,d)/C_R(r,d) = \exp\{(nF/RT)(E_s - E^{\circ\prime})\} \quad (11)$$

$$D_O[\partial C_O(r,z)/\partial z]_{z=d} + D_R[\partial C_R(r,z)/\partial z]_{z=d} = 0 \quad (12)$$

while for an insulating substrate

$$[\partial C_O(r,z)/\partial z]_{z=d} = [\partial C_R(r,z)/\partial z]_{z=d} = 0 \quad (13)$$

The potential in the substrate boundary condition, eq 11, will frequently be the equilibrium potential of the solution, i.e., $E_s = E_{eq}$, where

$$E_{eq} = E^{\circ\prime} + (RT/nF) \ln (C_O^*/C_R^*) \quad (14)$$

since most of the conductive substrate, which is assumed to be large compared to the tip diameter, will be in contact with bulk solution. This is very convenient experimentally, because in many cases the substrate will be too small or weak to allow the attachment of a suitable electrical contact.

To our knowledge, this set of equations cannot be solved analytically. Before a digital simulation was carried out, they were cast in a dimensionless form by making the following substitutions:

$$R = r/a \quad (15)$$

$$Z = z/a \quad (16)$$

$$L = d/a \quad (17)$$

$$\mathrm{FCR}(R,Z) = C_R(r/a,z/a)/C_R^*$$

$$\mathrm{FCO}(R,Z) = C_O(r/a,z/a)/C_R^* \quad (18)$$

$$RG = r_{glass}/a \quad (19)$$

For simplicity, we assumed that $D_O = D_R = D$ and that the bulk solution contained only species R (i.e., $C_O^* = 0$ and $E_{eq} \ll 0$). We also treat the case where E_d is sufficiently positive that R is oxidized to O at the disk at a mass transfer controlled rate, i.e., $C_R(r,0) = 0$ for $0 \leq r \leq a$. Under these conditions

$$C_O(r,z) = C_R^* - C_R(r,z) \quad (20)$$

and only the differential equation for R needs to be simulated, with $C_O(r,z)$ then immediately obtainable from eq 20. The simulation must then solve the following set of dimensionless equations:

$$\partial^2\mathrm{FCR}(R,Z)/\partial R^2 + (1/R)(\partial\mathrm{FCR}(R,Z)/\partial R) + \partial^2\mathrm{FCR}(R,Z)/\partial z^2 = 0 \quad (21)$$

$$\mathrm{FCR}(R,0) = 0 \quad (Z = 0 \text{ and } 0 \leq R \leq 1) \text{ (disk electrode surface)} \quad (22)$$

$$\partial\mathrm{FCR}(R,Z)/\partial Z = 0 \quad (Z = 0 \text{ and } 1 < R \leq RG) \text{ (glass sheath)} \quad (23)$$

$$\mathrm{FCR}(R,Z) = 1 \quad (0 < Z < L \text{ and } R \geq RG) \text{ (semiinfinite condition)} \quad (24)$$

and either

$$\mathrm{FCR}(R,L) = 1 \quad (Z = L \text{ and } R \geq 0) \text{ (conductive substrate)} \quad (25)$$

or

$$\partial\mathrm{FCR}(R,Z)/\partial Z = 0 \quad (Z = L \text{ and } R \geq 0) \text{ (insulating substrate)} \quad (26)$$

The boundary condition in eq 24 implies that for both types of substrate, the supply of R from the bulk is high beyond RG; the region is not blocked by the glass sheath around the tip even when the tip is close to the sample so that the concentration of R essentially remains at the bulk concentration.

The above set of equations are solved by the finite element method. It is beyond the scope of this paper to give a detailed treatment of the FEM and the programming procedures employed; a complete discussion can be found in ref 6 and 7. An outline of the approach and a description of the two-dimensional exponentially expanding grid method are given in the Appendix.

RESULTS AND DISCUSSION

Program Check and Error Analysis. To check the algorithms used, as described in the Appendix, and gauge the effect of grid size on the accuracy of the solutions obtained, the concentration profiles and current at the disk electrode were computed under semiinfinite boundary conditions, i.e., $RG = 1000$ and $L = 1000$, when the tip electrode is very far from the substrate. This problem has already been treated by Newman (*2*) and Saito (*3*) and yields the steady-state current given by eq 1. The resulting concentration profiles are shown in Figure 3A. The errors in the calculated current as a function of choice of grid size parameters DREL, DRGL, and DZEL (see Appendix) are shown in Figure 4. This error is less than 1% for the following range of grid parameters: $0.0001 < \mathrm{DREL} < 0.001$; $0.0001 < \mathrm{DRGL} < 0.001$; $0.0005 < \mathrm{DZEL} < 0.002$. The accuracy of calculations made with smaller values of L (i.e., with the tip nearer the substrate) should be at least as good, because the exponential grid factor, b, employed is smaller than that used for the semiinfinite simulation and the number of grid elements employed is the same. Thus, parameters within these ranges were used for all simulations with smaller L values. We should emphasize the utility of using the exponentially expanding grid approach in being able to carry out this simulation. If a linear grid with a spacing of 0.01 would be employed, for example, then a few hundred grid elements in both the Z and R directions would be needed to obtain a 1% accuracy. An unreasonably large memory would be needed for the simulation. For example, a 1000×1000 grid simulation by the FEM would require the solution of a $10^6 \times 10^6$ square matrix and use about 16 Gbytes of memory!

Conductive Substrates. Simulations with the tip approaching a planar substrate were carried out for different values of tip/substrate distance (L) and size of the glass sheath surrounding the tip (RG). Typical concentration profiles for $L = d/a = 1$ are shown in Figure 3B. The increase in concentration of R in the vicinity of the electrode caused by the feedback effect compared to that under semiinfinite conditions (Figure 3A) is clearly shown. The current at the disk electrode is obtained by summation of the fluxes of R, proportional to the concentration gradients at $z = 0$ for $0 \leq r \leq a$. Values of the tip current, normalized to that at long distance, are given in Figure 5 and Table II. The tip current with a conductive substrate is the same for $RG = 100$ or 1000 and thus should not strongly depend on the size of the glass sheath surrounding the disk. An approximate (within 2%) analytical equation that fits the simulated results is

$$(i_T/i_\infty) = (\pi/4)(a/d) + 0.901 + 0.099 \exp[-0.16(a/d)] - 0.29 \exp[-0.39(d/a)] \quad (27)$$

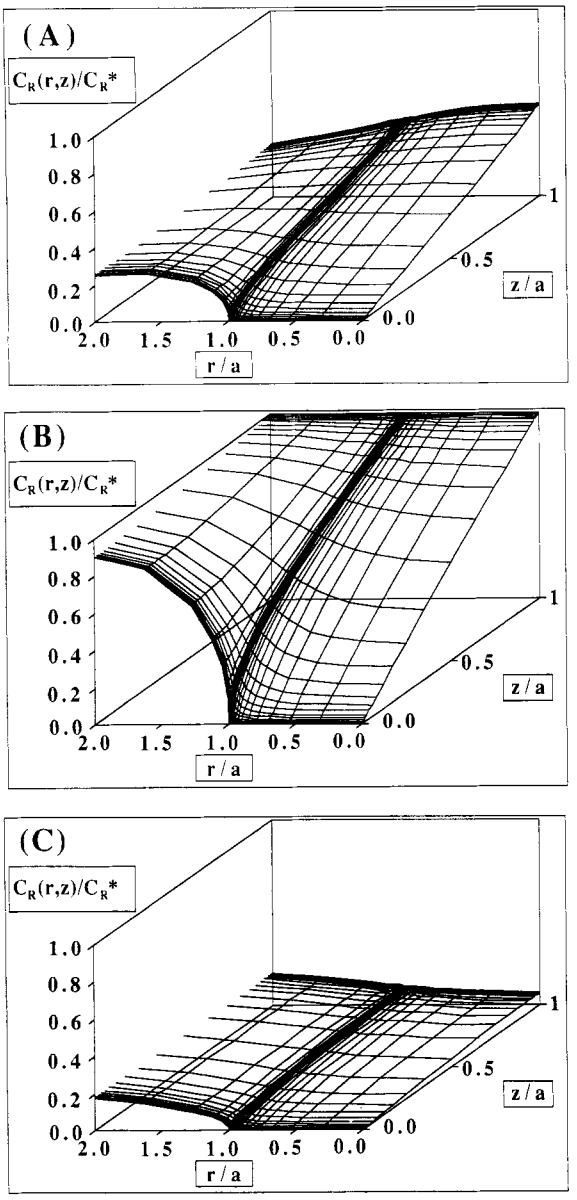

Figure 3. Computed concentration profiles at different substrates: (A) semiinfinite boundary condition (far from substrate), (B) conductive substrate at $L = d/a = 1$ (calculation conditions: NREL = NZEL = 18, NRGL = NZSUB = 19, DREL = DRGL = DZEL = DZSUB = 0.005, $L' = L/2$, RG = 1000), (C) insulating substrate at $L = 1$ (same calculation conditions as in B).

where i_∞ is the tip current when $d \rightarrow \infty$. In our previous paper (*1*) we pointed out that the feedback effect in the limit of small d should approach that of a thin-layer cell, where the current is given by $nFAD_RC_R^*/d$. This proportionality of i_T with $1/d$ is shown in Figure 6. Also given in Figure 6 are experimental points for the oxidation of ferrocene (Fc) to Fc^+ at a 5 μm radius tip electrode above a Pt substrate immersed in MeCN/25 mM TBABF4. The agreement between theory and experiment is excellent. Ideally, because the normalized tip current can be directly related to distance through the results in Table II, the SECM should allow absolute determinations of surface topography without calibration of the piezoelectric drive, when the disk radius is known. Deviations between actual and theoretical currents are expected, however, if the tip geometry deviates from the ideal disk-in-insulator arrangement assumed in the simulations.

Insulating Substrates. The calculated concentration profiles for the tip near the surface of an insulating substrate (with $L = d/a = 1$) are given in Figure 3C. Here the concentrations of R near the electrode surface are much smaller

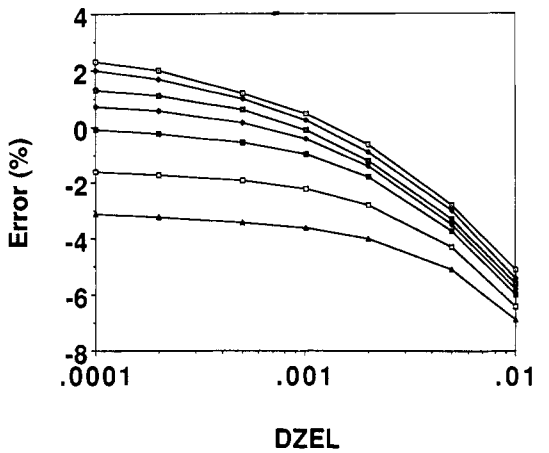

Figure 4. Error analysis for the semiinfinite boundary condition for different DZEL and DREL (calculation conditions: NZEL = 34, NZSUB = 3, NREL = 18, NRGL = 19, DZSUB = 1, DREL = DRGL): ⊡, DREL = 0.0001; ◆, DREL = 0.0002; ◘, DREL = 0.0005; ◇, DREL = 0.0010; ■, DREL = 0.0020; □, DREL = 0.0050; ♦, DREL = 0.0100.

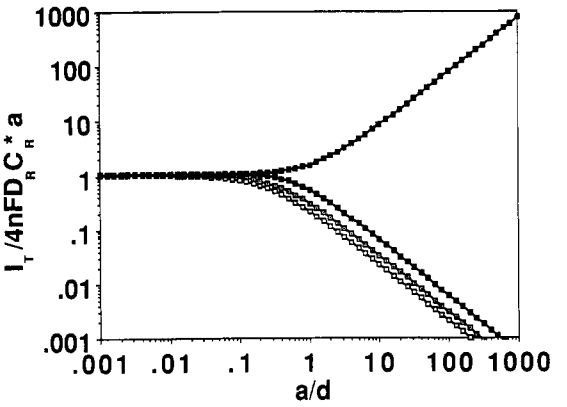

Figure 5. Normalized tip currents as functions of the substrate material and the inverse of the normalized tip/substrate distance. Calculation conditions were same as in Figure 3B except for the *RG* and *L* values: ■, *RG* = 1000 or 100 and the conductive substrate; ⊞, *RG* = 10 and the insulating substrate; ⊡, *RG* = 100 and the insulating substrate; □, *RG* = 1000 and the insulating substrate.

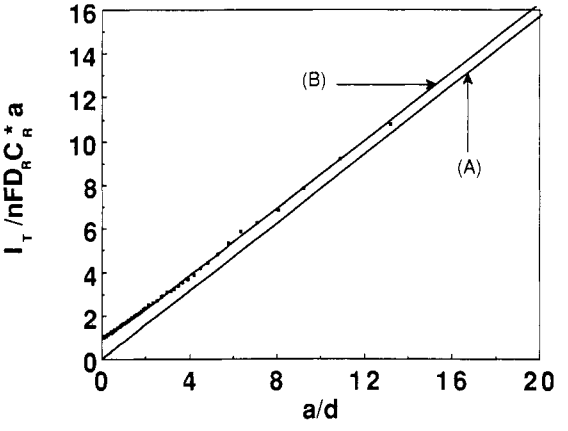

Figure 6. A comparison between theoretical and experimental results for a conductive substrate: curve A, thin layer theory; curve B, calculated, as in Figure 5; ■, experimental data (see text).

than those at long distance (Figure 3A) because of the blocking effect of the substrate. The calculated normalized tip current as a function of distance is shown in Figure 5 and Table II. As opposed to the results found with a conductive substrate, the current in this case depends upon the size of the glass sheath surrounding the tip (*RG* = 10, 100, 1000) and decreases as the sheath radius increases. This can be understood in terms of the increase in the blockage of diffusion to the disk

Table II. Normalized Tip Currents as Functions of the Substrate Material and the Tip/Substrate Distance[a]

	$I = I$(material, RG, L) = $i_T/nFD_RC_R{}^*a$				
	conductive substrate		insulating substrate		
log L	RG = 100	RG = 1000	RG = 10	RG = 100	RG = 1000
2.0	1.0158	1.0105	1.0563	1.0098	1.0018
1.9	1.0164	1.0106	1.0558	1.0088	0.9971
1.8	1.0173	1.0111	1.0553	1.0071	0.9909
1.7	1.0187	1.0122	1.0549	1.0045	0.9828
1.6	1.0205	1.0140	1.0544	1.0007	0.9722
1.5	1.0229	1.0164	1.0540	0.9951	0.9584
1.4	1.0260	1.0196	1.0535	0.9872	0.9407
1.3	1.0301	1.0237	1.0530	0.9760	0.9181
1.2	1.0355	1.0291	1.0523	0.9607	0.8899
1.1	1.0425	1.0361	1.0509	0.9402	0.8552
1.0	1.0515	1.0451	1.0479	0.9132	0.8132
0.9	1.0631	1.0569	1.0412	0.8785	0.7639
0.8	1.0783	1.0721	1.0285	0.8353	0.7075
0.7	1.0980	1.0919	1.0073	0.7832	0.6450
0.6	1.1237	1.1178	0.9750	0.7224	0.5781
0.5	1.1576	1.1518	0.9296	0.6545	0.5092
0.4	1.2022	1.1967	0.8700	0.5816	0.4407
0.3	1.2614	1.2561	0.7970	0.5068	0.3751
0.2	1.3401	1.3351	0.7134	0.4335	0.3145
0.1	1.4445	1.4398	0.6238	0.3645	0.2602
0.0	1.5825	1.5780	0.5337	0.3021	0.2129
−0.1	1.7635	1.7594	0.4482	0.2474	0.1728
−0.2	1.9989	1.9950	0.3709	0.2009	0.1393
−0.3	2.3027	2.2990	0.3034	0.1619	0.1117
−0.4	2.6918	2.6884	0.2461	0.1299	0.0893
−0.5	3.1877	3.1845	0.1984	0.1039	0.0712
−0.6	3.8167	3.8137	0.1593	0.0829	0.0567
−0.7	4.6142	4.6113	0.1274	0.0660	0.0450
−0.8	5.6204	5.6177	0.1017	0.0524	0.0357
−0.9	6.8918	6.8891	0.0809	0.0416	0.0283
−1.0	8.4959	8.4933	0.0643	0.0329	0.0224
−1.1	10.5217	10.5193	0.0509	0.0260	0.0177
−1.2	13.0648	13.0624	0.0403	0.0206	0.0140
−1.3	16.2817	16.2793	0.0318	0.0162	0.0110
−1.4	20.3250	20.3228	0.0251	0.0128	0.0087
−1.5	25.4310	25.4288	0.0198	0.0101	0.0068
−1.6	31.8514	31.8493	0.0156	0.0079	0.0054
−1.7	39.8134	39.8114	0.0123	0.0062	0.0042
−1.8	50.2376	50.2357	0.0096	0.0049	0.0033
−1.9	62.8570	62.8551	0.0076	0.0039	0.0026
−2.0	79.0570	79.0551	0.0060	0.0031	0.0021

[a] Calculation conditions were the same as in Figure 3B except for the RG and L values. $L = d/a$.

electrode through the thin gap between the insulating sheath and the insulating substrate as the length of this region increases. Thus, a determination of the distance and topography of an insulating substrate requires knowledge of both disk and insulator radii. A comparison of experimental and simulation results is given in Figure 7. In this experiment the solution and tip were the same as that with a conductive substrate and a silicon wafer was used as the insulating substrate. In this case while the expected trend in normalized current with distance is obtained, the currents are larger than expected. This reflects the fact that the tip did not have the ideal disk geometry as defined in simulation. The experimental tips used here were produced by sealing Pt wire in glass and then tapering the flat glass section around the tip to a conical shape by polishing with emery paper to reduce the size of the sheath to 10–50 times the disk radius and then with diamond paste. This is necessary to reduce the possibility of the overhanging glass insulator contacting the substrate when the tip approaches the sample. However, this polishing procedure can taper back the sheath somewhat and perhaps gives a slight hemispherical or conical shape to the disk itself. This would cause a greater flux to the disk surface and greater currents than those predicted by the ideal model simulations. Generally technical difficulties prevent tip preparation with mathematically definable geometry and micrometer precision, i.e., with well-defined glass sheath radii. We usually use a disk-in-glass configuration with as small an effective r_{glass} as possible to reduce the possibility of the overhanging glass insulator contacting the substrate when the tip approaches the sample. Note that, even with the best data shown in Figure 7, three deviating experimental data points for large a/d values (i.e., $a/d > 5$ or $d < 1$ μm) probably reflect the glass sheath touching the substrate.

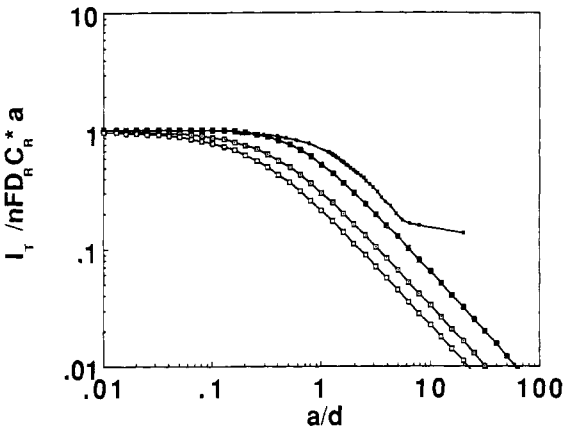

Figure 7. A comparison between theoretical and experimental results for an insulating substrate: ■, experimental data (see text); ⊞, RG = 10 and the insulating substrate; ⊡, RG = 100 and the insulating substrate; □, RG = 1000 and the insulating substrate.

In the case of insulating substrates, more rigorous boundary conditions reflecting the nonideal disk-in-glass geometry (i.e., a three-dimensional diffusion problem) as well as modification of the semiinfinite boundary conditions (eq 7–10) could be considered for a better agreement between experimental and theoretical results. Alternatively a technique that allows fabrication of tips with a geometry close to that of the model might be developed. Both of these approaches appear quite difficult, however.

CONCLUSIONS

The tip current for the SECM operating in the feedback mode and utilizing a disk-shaped electrode over a planar substrate has been calculated for both conductive and insulating samples by solving the steady-state diffusion equations by the FEM with an exponentially expanding grid. The theoretical curves for the normalized tip current vs tip/substrate distance are independent of the radius of the insulating glass sheath surrounding the disk and can be used to find the absolute tip/substrate distance. With an insulating sample, the results do depend upon the glass sheath radius and an empirical calibration curve is required for a given electrode to obtain the distance from the measured tip current. Although the theory developed here strictly applies only to a steady-state situation, it will be applicable to measurement where the tip is scanned over the sample in the x–y direction, as long as the scanning speed is slow compared to the time needed for the ultramicroelectrode tip to attain steady state. How slow a scanning speed is needed depends upon the size of the tip electrode and d, because a smaller disk electrode and one held very close to the substrate will reach steady state more rapidly than a larger disk at a long distance (*11–13*). Practically, the maximum speed for a given tip can be determined by scanning over the same sample with increasing speeds until a substantial difference is detected in the response. Note also that the above simulations apply to an essentially planar substrate, and that deviations from theoretical behavior could arise with substrate geometries that are substantially nonplanar (e.g., with sharp discontinuities or

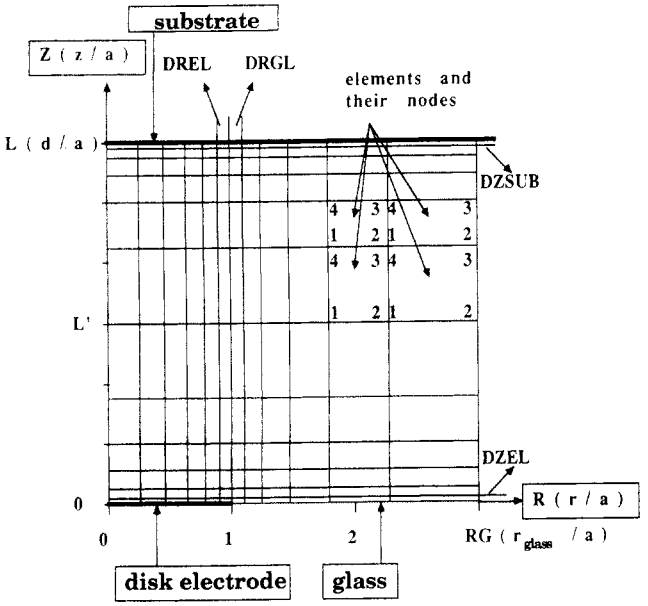

Figure 8. The two-dimensional exponential grids employed in the simulation where $L = 6$, $L' = 3$, $RG = 3$, NREL = NRGL = NZEL = NZSUB = 7, DREL = DRGL = DZEL = DZSUB = 0.1 and the element node numbering system.

hemispherical structures that are of the order of the tip radius).

APPENDIX

The dimensionless equations, eq 21–24 with either boundary condition, eq 25 or 26, were solved by the FEM. In this method the R, Z space is divided into a set of elements, each denoted by the superscript (e), as shown in Figure 8. The methods and notation generally follow those in references 6 and 7.

The field variable ($FCR^{(e)}(R,Z)$) in one element (e) of the space domain (a rectangle in the R,Z plane) is approximated by a set of four linear interpolation polynomials $N_j^{(e)}$ (bilinear Lagrange polynomials) which is 1 at one element node or one corner point, j, of the rectangle and 0 at the other nodes and also 0 outside the element domain, i.e.

$$FCR^{(e)}(R,Z) \cong \sum_{j=1}^{4} N_j^{(e)}(R,Z)\, FCR^{(e)}(R_j,Z_j) \quad \text{(A1)}$$

where (see Figure 8 for coordinate index)

$$N_j^{(e)}(R,Z) = \frac{1}{4}\left\{1 + \left(\frac{2R - R_3 - R_1}{R_3 - R_1}\right)\left(\frac{2R_j - R_3 - R_1}{R_3 - R_1}\right)\right\} \times \left\{1 + \left(\frac{2Z - Z_4 - Z_1}{Z_4 - Z_1}\right)\left(\frac{2Z_j - Z_4 - Z_1}{Z_4 - Z_1}\right)\right\} \quad \text{(A2)}$$

or using vector notation

$$FCR^{(e)}(R,Z) \cong \{N\}^{(e)}\{FCR\}^{(e)} \quad \text{(A3)}$$

where

$$\{N\}^{(e)} = \{N_1^{(e)}(R,Z), N_2^{(e)}(R,Z), N_3^{(e)}(R,Z), N_4^{(e)}(R,Z)\} \quad \text{(A4)}$$

$$\{FCR\}^{(e)} = \begin{Bmatrix} FCR^{(e)}(R_1,Z_1) \\ FCR^{(e)}(R_2,Z_2) \\ FCR^{(e)}(R_3,Z_3) \\ FCR^{(e)}(R_4,Z_4) \end{Bmatrix} \quad \text{(A5)}$$

The above element equations can be summed over all the space domain to obtain {FCR}, where

$$\{FCR\} = \begin{Bmatrix} FCR(R_{1'},Z_{1'}) \\ FCR(R_{2'},Z_{2'}) \\ FCR(R_{3'},Z_{3'}) \\ \cdots \\ \cdots \\ FCR(R_{n'},Z_{n'}) \end{Bmatrix} \quad \text{(A6)}$$

and the points $R_{j'},Z_{j'}$ are the nonduplicate points on the two-dimensional exponential mesh which is described later. Therefore, the global matrix equation is similar in form to eq A3, i.e.

$$FCR(R,Z) \cong \{N\}\{FCR\} \quad \text{(A7)}$$

where

$$\{N\} = \{N_{1'}(R,Z), N_{2'}(R,Z), N_{3'}(R,Z), \ldots, N_{n'}(R,Z)\} \quad \text{(A8)}$$

The resulting functions $N_{j'}(R,Z)$ ($j = 1, 2, \ldots, n$ and n is the total number of grid points) will be the specific summation of element interpolation polynomials $N_j^{(e)}(R,Z)$ that depend on the global grid and element numbering. These global interpolation polynomials will be 1 at the global node, j', and 0 at the other nodes and also 0 in the element domains which does not include the nodal point, j'.

So far, only the approximate field variable functions to be solved have been developed. Introducing the Bubnov–Galerkin method, where the weighing functions are chosen to be same as the approximating functions ($N_{j'}(R,Z)$), the equation to be solved is formulated, from eq 21

$$\int_{R=0}^{R=RG}\int_{Z=0}^{Z=L}\left[\{N\}^T\left(\frac{\partial^2 FCR(R,Z)}{\partial R^2} + \left(\frac{1}{R}\right)\frac{\partial FCR(R,Z)}{\partial R} + \frac{\partial^2 FCR(R,Z)}{\partial Z^2}\right)2\pi\, dR\, dZ\right] = \{0\} \quad \text{(A9)}$$

where $\{N\}^T$ is the transpose vector of {N}. A combination of eq A7 and A9 yields the integro-differential matrix equation

$$\int_{R=0}^{R=RG}\int_{Z=0}^{Z=L}\left[\{N\}^T\left(\frac{\partial^2\{N\}}{\partial R^2} + \left(\frac{1}{R}\right)\frac{\partial\{N\}}{\partial R} + \frac{\partial^2\{N\}}{\partial Z^2}\right)2\pi\, dR\, dZ\right]\{FCR\} = \{0\} \quad \text{(A10)}$$

Equation A10 is the matrix representation of the simultaneous *linear* equations, where the matrix elements do not contain any unknown variables, but the integration causes some complexity. However, some of the values of $FCR(R_{j'},Z_{j'})$ are already known from the boundary conditions at the boundary surfaces. Rearrangement of the eq A10 to include these boundary conditions results in nonsingular matrix equations with a nonzero vector as the right-hand side of eq A10. This procedure is explained on page 51 in the ref 6. After this rearrangement, the square matrix (n by n, where n is the total number of grid points) can be recognized as a band matrix the size of which is dependent on the total number of R directional grids (n_R) or that of Z directional grids (n_Z), i.e., $n_R + 2$ or $n_Z + 2$. The rearranged form of eq A10 is evaluated on the computer, by numerical integration and inversion of the band matrix (n by $n_R + 2$ or n by $n_Z + 2$). For the numerical integration, the Gauss–Legendre quadrature method (*6*) was used.

To specify the global nodal points that are spread on the R,Z plane, the exponentially expanding grid method (*8–10*) was used. This method is critical to solution of this problem, because practically the size of computer memory is finite and

a relatively large memory is essential for the inversion of the matrix. Four directions of exponentially expanding grids (Figure 8) were used to increase the accuracy. From the principle that the region of steeper concentration gradients has to provide more grids than the other regions, four directional expanding grids were selected as follows: first, NZEL grids from $Z = 0$ to $Z = L'$ starting with a DZEL grid size, where $0 < L' < L$; second, NZSUB grids from $Z = L$ to $Z = L'$ starting with a DZSUB grid size; third, NREL grids from $R = 1$ to $R = 0$ starting with a DREL grid size; fourth, NRGL grids from $R = 1$ to $R = RG$ starting with a DRGL grid size.

The above formulation, including automatic two-dimensional exponential grid generation, was coded in FORTRAN and executed on either a CDC 6000 dual cyber computer (Control Data Corp.) or a Macintosh II (Apple Computer, Inc). To obtain one data point in Figure 5, took 35 s on the CDC 6000 and 390 s on the Macintosh II. The needed number of bytes of memory largely depended on the size of band matrix and inverted band matrix, i.e., the number of memory bytes $= 8 \cdot 2 \cdot n \cdot (n_R + 2)$ or $8 \cdot 2 \cdot n \cdot (n_Z + 2)$, where 8 bytes were used for each floating point number.

Once the steady-state concentration profiles were obtained, the current at the disk electrode was easily calculated by the summation of the normal components of the concentration gradient.

LITERATURE CITED

(1) Bard, A. J.; Fan, F.-R. F.; Kwak, J.; Lev, O. *Anal. Chem.* **1989**, *61*, 132-138.
(2) Newman, J. *J. Electrochem. Soc.* **1966**, *113*, 501-502.
(3) Saito, Y. *Rev. Polarogr.* **1968**, *15*, 177-187.
(4) Feldberg, S. W. In *Electroanalytical Chemistry*; Bard, A. J., Ed.; Marcel Dekker: New York, 1969; Vol. 13.
(5) Feldberg, S. W. In *Computers in Chemistry and Instrumentation*; Mattson, J. S., Mark, H. B., MacDonald, H. C., Jr., Eds.; Marcel Dekker: New York, 1972; Vol. 2.
(6) Huebner, K. J.; Thornton, E. A. *The Finite Element Method for Engineers*, 2nd ed.; Wiley-Interscience: New York, 1982.
(7) Rao, S. S. *The Finite Element Method in Engineering*; Pergamon Press: New York, 1982.
(8) Joslin, T.; Pletcher, D. *J. Electroanal. Chem.* **1974**, *49*, 172-186.
(9) Feldberg, S. W. *J. Electroanal. Chem.* **1981**, *127*, 1-10.
(10) Bard, A. J.; Crayston, J. A.; Kittlesen, G. P.; Varco Shea, T.; Wrighton, M. S. *Anal. Chem.* **1986**, *58*, 2321-2331.
(11) Aoki, K.; Osteryoung, J. *J. Electroanal. Chem.* **1981**, *122*, 19-35.
(12) Shoup, D.; Szabo, A. *J. Electroanal. Chem.* **1982**, *140*, 237-245.
(13) Hubbard, A. T.; Anson, F. C. In *Electroanalytical Chemistry*; Bard, A. J., Ed.; Marcel Dekker: New York, 1970; Vol. 4.

RECEIVED for review December 9, 1988. Accepted March 1, 1989. The support of this research by the Robert A. Welch Foundation is gratefully acknowledged.

Continuous Liquid-Phase Piezoelectric Biosensor for Kinetic Immunoassays

Kenneth A. Davis*[1]

Department of Pediatrics, RD-20, University of Washington, Seattle, Washington 98195

T. Richard Leary

National Biosensor, 20212 Densmore North, Seattle, Washington 98133

The reactions of immunoglobulins with protein A and, subsequently, of antibodies to these immunoglobulins were continuously monitored by a piezoelectric biosensor. AT-cut crystals, with a fundamental resonant frequency of 10 MHz, were mounted in a Plexiglas holder, and one side was directly coated with protein A. Upon exposure to solutions containing rabbit or human IgG the resonant frequency was followed continuously and its decrease due to the binding of IgG to protein A observed. Subsequent addition of sheep antihuman IgG to the now immobilized human IgG caused a specific 3-fold further decrease in resonant frequency. We observed a frequency change of approximately 1 Hz for each 10 ng of added immunoglobulin. Decreasing the pH to 3 released the bound IgG but not the protein A and permitted reuse of the crystal for further IgG binding.

Increasing attention is being paid to the development of nonelectrode biosensors, especially those that can be used to determine clinically important molecules (*1*, *2*). These sensors are constructed by immobilizing a selective binding surface to a transducer. The surface can be an absorptive organic film, an immobilized antigen, an immobilized antibody against a specific antigen, or other proteins with specific binding sites. Selective binding of a molecule to the absorptive surface causes the transducer to change one or more of its fundamental signals.

The piezoelectric quartz crystal is such a transducer and is commonly used as a low-cost frequency standard. The crystal oscillates at a very specific resonant frequency when placed in an appropriate circuit. The frequency of this resonance can be changed by adding mass to the surface of the crystal.

Some biological applications of quartz crystal microbalances have been reported. Quartz crystals have been coated with antibodies to the pesticide parathion and have been used to specifically detect parathion in gases that are passed over the crystal (*3*). Shons et al. (*4*) used antigen-coated crystals exposed to specific antisera and demonstrated a mass increase after washing and drying. Similarly, Muramatsu et al. (*5*) have detected specific mass changes of air-dried crystals coated with monoclonal antibodies to the yeast *Candida albicans* before and after incubation with suspensions of *C. albicans*. Recently, Muramatsu et al. (*6*) have reported the coupling of protein A to 9-MHz AT-cut crystals with (γ-aminopropyl)-triethoxysilane. They measured IgG binding by observing the change in resonant frequency of a crystal immersed in distilled

[1] Present address: Becton Dickinson Monoclonal Center, 2375 Garcia Ave., Mountain View, CA 94043.

0003-2700/89/0361-1227$01.50/0 © 1989 American Chemical Society